Oikos

o19735

Perez-Heydrich, C., Oli, M. K. and Brown, M. B. 2012. Population-level influence of a recurring disease on a long-lived wildlife host. – Oikos 121: 377–388.

Appendix A1

Methods for the estimation of demographic parameters

Capture and sampling of tortoises

All field protocols were fully approved by the Univ. of Florida IACUC. Census surveys were conducted at the three study sites (BS, FE, OR; Fig. A1) to locate active and inactive burrows. Burrows were mapped with a GPS device, and flagged according to size class, as determined from burrow width and depth measurements. Bucket traps were placed at the mouth of burrows randomly selected according to size class and activity status, and traps were checked daily for captures. The trapping methodology utilized depended on the size class of the burrow being trapped, with one gallon buckets used for juveniles and hatchlings (burrow width ≤ 155 mm in diameter), five gallon buckets used for subadult and adult burrows (155<burrow width <320), and 10 gallon buckets for large adult burrows (burrow width ≥ 320 mm). Holes were drilled in all buckets for water drainage, and shade covers made out of vinyl siding were placed over the traps to protect the tortoises from overheating.

Blood samples and nasal flushes were collected from each captured tortoise for determination of *M. agassizii* infection status as indicated by ELISA and PCR results (Brown 2002, Wendland et al. 2007). Morphometric measurements and complete health assessments were performed on each tortoise. Tortoises were sexed based on degree of plastral concavity and aged according to the count of plastral

rings (Germano 1988). Radiographs were obtained from adult females to determine the presence of eggs and clutch size. After data collection, tortoises were returned to the burrow from which they were captured.

Parameter estimation

Stage-specific survival probabilities (σ_H, σ_P, σ_R)

Capture histories spanning the 2003–2006 sampling period were generated for each tortoise from each study site. We used multistate capture-mark-recapture (CMR) to estimate and model stage-specific annual apparent survival and capture probabilities from the individual capture histories (Amstrup et al. 2005, McDonald 2008, Williams et al. 2001). For all models, annual apparent survival probability (*s*) was allowed to vary only by stage class, whereas annual capture probability (*c*) could vary by stage, year, or site, depending on the model. Stages were defined as 'pre-reproductive' (carapace length < 220 mm) and 'reproductive' (carapace length ≥ 220 mm). Akaike information criterion corrected for small sample size (AICc) were used to compare competing models in the set for model comparison and statistical inference (Burnham et al. 2002, p. 150). Two models provided equally adequate fits to the data (difference in AICc, ΔAICc = 0.032), whereas all others fit the data poorly (ΔAICc > 10.0); thus, we used model-averaged estimates of stage-specific survival to parameterize the baseline population (i.e. disease free) projection matrix (Table A1). Model-averaged estimates were obtained using the following equation (Burnham et al. 2002, p. 150):

$$\tilde{\theta} = \sum_{i=1}^{R} w_i \hat{\theta}_i ,$$

where R represents the number of models being averaged across, w_i represents the model-specific Akaike weight, and θ_i represents the model-specific parameter estimate. The unconditional variance of the model-averaged estimate was calculated as (Burnham et al. 2002, p. 162):

$$\overline{v}\left(\tilde{\theta}\right) = \sum_{i=1}^{R} w_i \sqrt{\overline{v}\left(\hat{\theta}_i \mid g_i\right) + \left(\hat{\theta}_i - \tilde{\theta}\right)^2} \ ,$$

where g_i represents the specific model used to estimate the parameter $\hat{\theta}_i$.

Pre-reproductive growth probability (γ)

Because gopher tortoises grow very slowly, probability of growing from pre-reproductive to reproductive state could not be estimated from the CMR data. Thus, the probability of growth from the pre-reproductive to the reproductive stage was estimated using the fixed stage duration approach described by Caswell (2001):

$$\gamma = \frac{\left(\frac{\sigma}{\lambda}\right)^T - \left(\frac{\sigma}{\lambda}\right)^{T-1}}{\left(\frac{\sigma}{\lambda}\right)^T - 1} \qquad \text{(A1)}$$

The fixed stage duration (T) was obtained by first fitting a von Bertalanffy curve to age-size data from the pooled study populations (i.e. individuals pooled from all study sites), with plastral ring counts used to represent a tortoise's age in years (Berry 2002, Germano 1988, Mushinsky et al. 1994, Wilson et al. 2003). Maximum likelihood parameter estimates from the von Bertalanffy growth curve were then used for the inverse prediction of age at 220 mm carapace length, since this was the size used to delineate pre-reproductive and reproductive stage classes (Fig. A2). The age of a tortoise at 220 mm represents the length of time a tortoise spends in the pre-reproductive stage, and therefore the fixed stage duration (T) of pre-reproductive tortoises. Using this value of T (7.278 years, 95CI: 2.982–11.573) along with the annual survival probability of pre-reproductive tortoises (σ_P) obtained from the CMR analysis as described above, the growth probability of this stage class (γ) was calculated using Eq. A1 assuming

$\lambda = 1$. This method has been used to estimate stage-specific growth probabilities for other turtle populations (Crouse, et al. 1987).

Fecundity (m)

Annual fecundity rate was calculated from clutch size (*cs*), proportion of females gravid (*pg*), nest success probability (*ns*) and hatch success rate (*hs*). Mean clutch size and proportion of gravid females were obtained from radiographs of adult females sampled from the pooled study populations prior to oviposition. Estimates of nest and hatch success were derived from published studies because these parameters were not directly measured from our study populations. However, rather than adopting the results of a single study to quantify either parameter, two separate meta-analyses were conducted that pooled the results of all available studies that measured nest and/or hatch success across different gopher tortoise populations (Perez-Heydrich 2010).

The data for the meta-analyses were obtained through a literature search using the Web of Knowledge database for all years. For the nest success meta-analysis, a total of 12 published studies were identified through the search, but after reviewing titles and abstracts, only 5 were relevant. Of these five studies, none provided an actual estimate of nest depredation rates. The cited literature from these studies was then further investigated. Three studies that quantified nest success in natural populations were finally identified (Landers et al. 1980, Wright 1982, Marshall 1987). The same process was followed for hatch success rate data, which identified seven studies that provided useful data for the hatch success meta-analysis (Brode 1959, Landers et al. 1980, Krebs et al. 1995, Butler et al. 1996, Epperson et al. 2003, Pike et al. 2006).

Effect sizes for each study were defined as proportions (*p*), and standard errors of these proportions were calculated using the equation (Lipsey et al. 2001):

$$\sqrt{\frac{p(1-p)}{n}} \tag{A-2}$$

where *n* represents the study-specific sample size. For the nest success meta-analysis *n* was the total number of nests monitored for each study, but for the hatch success meta-analysis *n* represented the total number of eggs monitored in each study. The summary estimates of nest and hatch success that resulted from these meta-analyses were expected to be less biased representations of these parameters in an average gopher tortoise population, as these parameters varied substantially across studies and populations (Fig. A3; tests of heterogeneity, $Q_{ns} = 11.98$, DF = 2, p = 0.003; $Q_{hs} = 521.86$, DF = 6, p = 0.000).

The composite annual fecundity rate *m* was then calculated as the product of its components ($m = (cs \times pg \times ns \times hs) / 2$). The variance of *m* was calculated using the delta method.

Table A1. Stage-specific annual apparent survival rates obtained from the multistate capture–mark–recapture (CMR) analysis of data collected from a four-year CMR study of gopher tortoises from historically URTD-free populations (BS, FE and OR; Fig. A1). Under the 'Model' column, *c*(*i*) corresponds to capture probability as a function of *i* covariates, and *s* to survival probability, which was a function only of stage class. Values in parenthesis represent the 95% Wald confidence intervals for model-specific estimates of apparent survival rates.

Model	ΔAICc	Deviance	Pre-reproductive survival	Reproductive survival
c(stage+year+site)*s(*stage)	0.000	546.188	0.408 (0.016–0.967)	0.902 (0.624–0.981)
c(year+site), *s(*stage)	0.032	546.221	0.368 (0.084–0.789)	0.903 (0.625–0.981)
c(site), *s(*stage)	10.521	546.417	0.377 (0.087–0.794)	0.910 (0.663–0.981)
c(stage +site), *s(*stage)	12.591	546.384	0.418 (0.016–0.970)	0.910 (0.662–0.981)
c(stage+year), *s(*stage)	23.175	569.363	0.730 (0.000–1.000)	0.881 (0.601–0.973)
c(year), *s(*stage)	24.430	570.619	0.336 (0.076–0.756)	0.886 (0.595–0.976)
c(.), *s(*stage)	28.634	570.750	0.343 (0.081–0.756)	0.893 (0.697–0.968)
c(stage), *s(*stage)	29.423	569.480	0.740 (0.000–1.000)	0.888 (0.635–0.973)
Model-averaged estimates	NA	NA	0.388 (0.037–0.913)	0.902 (0.634–0.981)

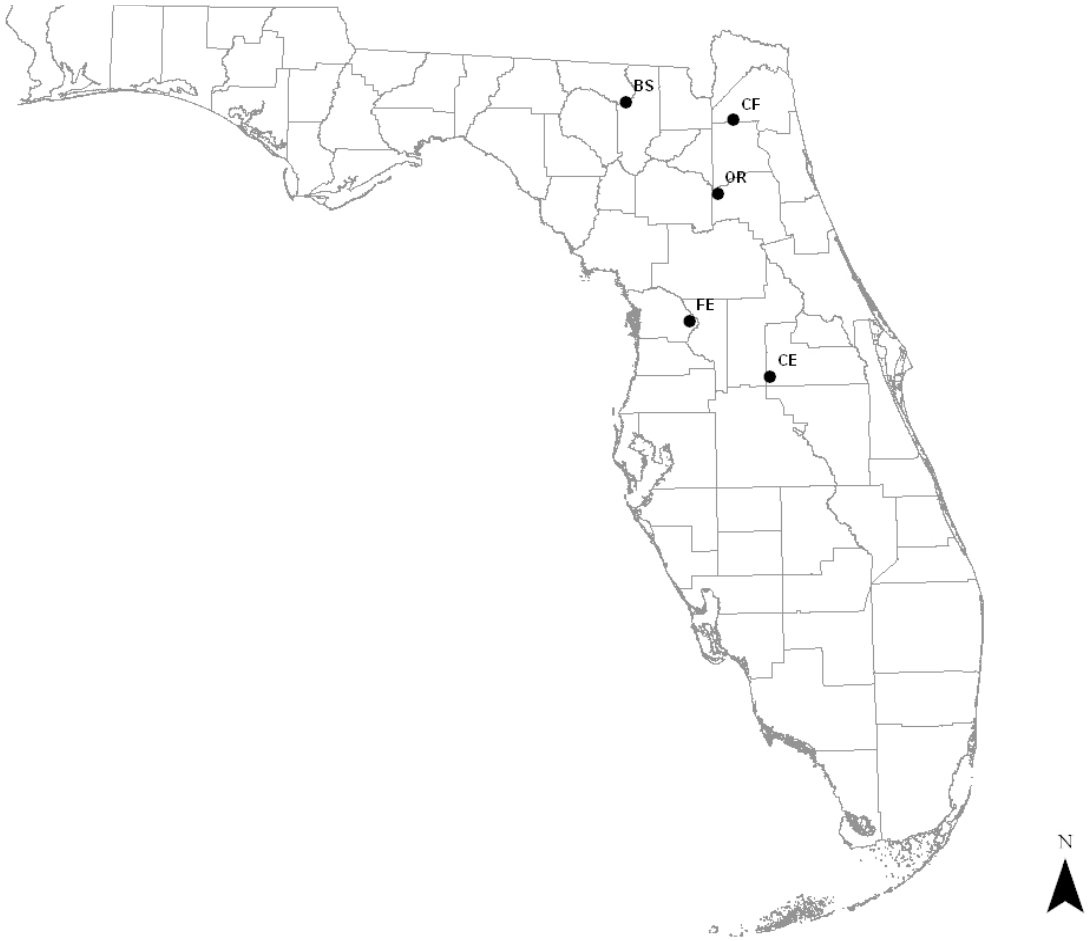

Figure A1. Location of study populations in Florida, USA. The study sites are represented by initials and include: Big Shoals State Park (BS), Flying Eagle Wildlife Management Area (FE), Ordway-Swisher Biological Station (OR), Branan Field Mitigation Park (CF), and a privately-owned tract of land in central Florida (CE).

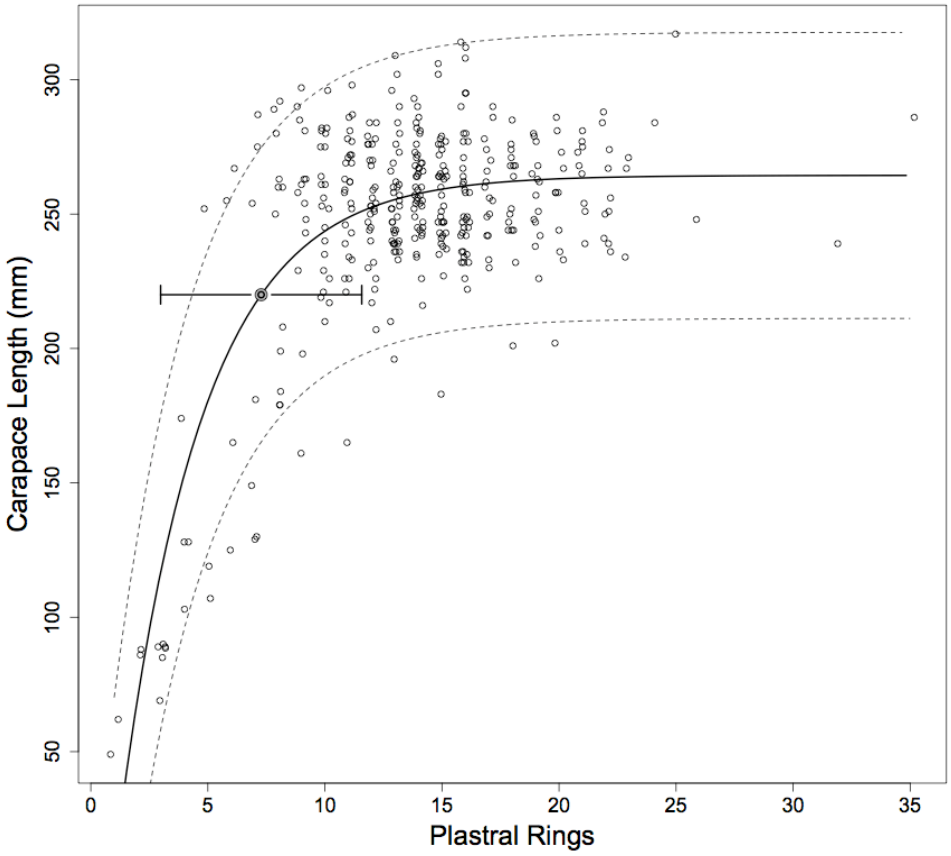

Figure A2. The von Bertalanffy growth curve (solid line) of gopher tortoises from historically URTD-free populations (BS, FE and OR); dotted lines represent 95% confidence limits. The grey point on the plot represents the mean age of tortoises that measure 220 mm in carapace length, with lines extending to the 95% confidence limits of this value (7.278 years; 95CI: 2.982–11.573), and represents the time a tortoise spends in the pre-reproductive stage (*T*).

Appendix A2

Methods for the calculation of stochastic and deterministic elasticities

Stochastic elasticities were calculated using the following equation (Caswell 2001):

$$\frac{d\log\lambda_S}{d\log a_{ij}} = \frac{1}{T}\sum_{t=0}^{T-1}\frac{v_{t+1}w'_t \circ A_t}{R_t v'_{t+1} w_{t+1}},$$

where w is the population structure vector, v is the reproductive value vector, a prime (‘) indicates transpose and a ‘o’ represents the Hadamard product. A sequence of T = 50 000 population states (endemic/epizootic) was generated according to probabilities assigned by a given Markovian transition matrix. From this simulated sequence of environments, a sequence of 50 000 population projection matrices ($A_0, A_1, \ldots A_{49999}$) was then generated in which A_t corresponded to the simulated disease state at time t. Assuming an arbitrary non-negative initial population structure vector (w_0) whose scalar product was 1, a sequence of w vectors and population growth rates (R_t) was created such that $w_{t+1} = \frac{A_t w_t}{\|A_t w_t\|}$, and $R_t = \|A_t w_t\|$. Likewise, assuming an arbitrary initial non-negative reproductive value vector (v_0) whose scalar product was also 1, another sequence of vectors was generated from the sequence of population projection matrices, whereby $v'_{t-1} = \frac{v'_t A_{t-1}}{\|v'_t A_{t-1}\|}$.

Elasticities from deterministic conditions were calculated using the vec permutation approach developed for the matrix metapopulation (Hunter et al. 2005). The ‘patches’ under this framework corresponded to endemic and epizootic population states. Demography within each patch was described by the population projection matrix specific to endemic and epizootic population dynamics, respectively:

$$\mathbf{B} = \begin{pmatrix} B_{Enzootic} & 0 \\ 0 & B_{Epizootic} \end{pmatrix},$$

where *i* represents one of the six levels of disease-induced mortality μ associated with a given epizootic condition. Dispersal between patches was held constant across all demographic stages(indicated by subscripts; *H* and *P* indicate hatchling and pre-reproductive, and R^- and R^+ sero-negative and sero-positive adults, respectively), and was therefore described by the same Markov chain model (P_j) for all four stages:

$$\mathbf{M} = \begin{pmatrix} M_H & 0 & 0 & 0 \\ 0 & M_P & 0 & 0 \\ 0 & 0 & M_{R-} & 0 \\ 0 & 0 & 0 & M_{R+} \end{pmatrix},$$

where $M_H = M_P = M_{R-} = M_{R+} = P_j$, and *j* here represents a specific combination of *f* (frequency of recurring epizootics) and ρ (duration of recurring epizootics) values that generated each of the nine Markovian transition matrices used in the analysis (details in the text).

Demography was assumed to occur after dispersal so that the force of infection (ϕ) and survival of reproductive adults (σ_R) would depend on whether the population was experiencing normal conditions or had transitioned to outbreak conditions. The metapopulation projection matrix was then calculated as **A = BV'MV'**, where **B** represents the block-diagonal demography matrix, **M** is the block-diagonal dispersal matrix, and **V** is the vec-permutation matrix (Hunter et al. 2005). The corresponding sensitivity matrices for demographic and dispersal transitions were calculated as $\mathbf{S_B = S_A V'M'V}$ and $\mathbf{S_M = VB'S_A V'}$, respectively, where S_A represents the sensitivity matrix for the metapopulation projection matrix *A*. Elasticities of λ_A to **B** and **M** were calculated as $E_B = \frac{1}{\lambda_A} B \circ S_B$ and $E_M = \frac{1}{\lambda_A} M \circ S_M$, respectively. In total, 54 metapopulation projection matrices were constructed to represent each type of outbreak scenario as defined by values of ρ, *f* and μ (disease-induced mortality).

For each metapopulation projection matrix, elasticity of λ to lower-level outbreak-associated

parameters (i.e., ρ and f), disease-associated parameters (i.e. μ and ϕ) and demographic parameters (i.e. σ_H, σ_P, σ_R, γ and m) were calculated as follows:

$$e_{\rho} = \frac{\rho}{\lambda} \sum_{ij} \frac{\partial \lambda}{\partial m_{ij}^{(k)}} \frac{\partial m_{ij}^{(k)}}{\partial \rho}$$

$$e_{f} = \frac{f}{\lambda} \sum_{ij} \frac{\partial \lambda}{\partial m_{ij}^{(k)}} \frac{\partial m_{ij}^{(k)}}{\partial f}$$

$$e_{\mu} = \frac{\mu}{\lambda} \sum_{ij} \frac{\partial \lambda}{\partial b_{ij}^{(k)}} \frac{\partial b_{ij}^{(k)}}{\partial \mu}$$

$$e_{\phi} = \frac{\phi}{\lambda} \sum_{ij} \frac{\partial \lambda}{\partial b_{ij}^{(k)}} \frac{\partial b_{ij}^{(k)}}{\partial \phi}$$

$$e_{\sigma_H} = \frac{\sigma_H}{\lambda} \sum_{ij} \frac{\partial \lambda}{\partial b_{ij}^{(k)}} \frac{\partial b_{ij}^{(k)}}{\partial \sigma_H}$$

$$e_{\sigma_P} = \frac{\sigma_P}{\lambda} \sum_{ij} \frac{\partial \lambda}{\partial b_{ij}^{(k)}} \frac{\partial b_{ij}^{(k)}}{\partial \sigma_P}$$

$$e_{\sigma_R} = \frac{\sigma_R}{\lambda} \sum_{ij} \frac{\partial \lambda}{\partial b_{ij}^{(k)}} \frac{\partial b_{ij}^{(k)}}{\partial \sigma_R}$$

$$e_{\gamma} = \frac{\gamma}{\lambda} \sum_{ij} \frac{\partial \lambda}{\partial b_{ij}^{(k)}} \frac{\partial b_{ij}^{(k)}}{\partial \gamma}$$

$$e_{m} = \frac{m}{\lambda} \sum_{ij} \frac{\partial \lambda}{\partial b_{ij}^{(k)}} \frac{\partial b_{ij}^{(k)}}{\partial m}$$

where $m_{ij}^{(k)}$ and $b_{ij}^{(k)}$ represent elements within the *kth* block-diagonal matrix within **M** and **B**, respectively. Lower-level elasticities associated with ρ and f were summed across stages, while those associated with μ and ϕ were summed across patches, in order to show the overall effect of these parameters on λ.

Appendix A3

Methods used to evaluate the effect of parametric uncertainty on estimates of quasi-extinction parameters

In order to quantify effects of uncertainties associated with estimates of demographic and disease parameters on quasi-extinction parameters, we used a parametric bootstrapping approach. For each of the 5000 simulations of 50 time steps (i.e. 50 years), we sampled demographic and disease parameters from appropriate statistical distributions. Statistical distributions and relevant parameters used for sampling each vital rate are given below:

Vital rate	Symbol	Estimate	Variance	Distribution	Parameters
Hatchling survival	σ_H	0.13	0.0014	Beta	$\alpha = 9.846383$ $\beta = 67.291943$
Fecundity	m	0.50	0.0874	Exponential	$\lambda = 0.50$
Pre-reproductive survival	σ_P	0.39	0.12	Normal	$\mu = -0.4537263$ $\sigma = 1.4321218$
Pre-reproductive growth	γ	0.001614	0.000076	Beta	$\alpha = 0.03259324$ $\beta = 20.16699123$
Reproductive survival	σ_R	0.90	0.0059	Normal	$\mu = 2.2176396$ $\sigma = 0.8735094$
Force of infection	ϕ	0.22	0.0016	Normal	$\mu = -2.161308$ $\sigma = 0.1611744$

Parameters for the above distributions were defined empirically. Because hatchling survival and pre-reproductive growth probabilities are constrained between zero and one, we used beta distributions to generate random values of these variables in our simulations. Specifically, parameters for beta-distributed demographic variables were calculated using the estimated means ($\bar{x}$) and variances (v)

obtained from previous analyses and the following equations: $\alpha = \bar{x}\left(\frac{\bar{x}(1-\bar{x})}{v} - 1\right)$ and $\beta = (1-\bar{x})\left(\frac{\bar{x}(1-\bar{x})}{v} - 1\right)$. We assumed values for fecundity followed an exponential distribution, since the only constraint for this variable was that it be greater than or equal to zero. The estimated mean of fecundity was used as the defining parameter of the exponential distribution. Survival of pre-reproductive and reproductive individuals, and force of infection were originally estimated using capture-mark-recapture analyses. Because we had the raw, untransformed logit-regression parameters available from these past analyses, we simulated these raw values assuming a normal distribution defined by the corresponding regression parameter estimates and standard errors. The sampled values were then back-transformed using an inverse logit transformation to provide estimates suitable for the corresponding population projection matrix.

Appendix A4

Table A3. Stochastic growth rates and 95% confidence intervals obtained using Tuljapurkar's small noise approximation for each of the 54 epizootic scenarios.

		μ					
ρ	f	0.01	0.05	0.1	0.15	0.2	0.3
–0.1	0.1	0.902 (0.895–0.908)	0.898 (0.865–0.931)	0.893 (0.827–0.96)	0.888 (0.788–0.989)	0.884 (0.749–1.018)	0.881 (0.731–1.031)
	0.2	0.901 (0.892–0.91)	0.893 (0.849–0.938)	0.884 (0.793–0.974)	0.874 (0.735–1.013)	0.864 (0.676–1.052)	0.859 (0.65–1.069)
	0.3	0.9 (0.89–0.91)	0.889 (0.838–0.94)	0.875 (0.769–0.98)	0.86 (0.696–1.024)	0.845 (0.62–1.07)	0.838 (0.586–1.09)
0.40	0.1	0.902 (0.895–0.908)	0.898 (0.865–0.931)	0.893 (0.827–0.96)	0.888 (0.788–0.989)	0.884 (0.749–1.018)	0.881 (0.731–1.031)
	0.2	0.901 (0.892–0.91)	0.893 (0.849–0.938)	0.884 (0.793–0.974)	0.874 (0.736–1.013)	0.864 (0.676–1.052)	0.86 (0.65–1.069)
	0.3	0.9 (0.89–0.91)	0.889 (0.838–0.94)	0.875 (0.769–0.98)	0.86 (0.696–1.024)	0.845 (0.62–1.07)	0.838 (0.586–1.09)
0.73	0.1	0.902 (0.895–0.908)	0.898 (0.865–0.931)	0.893 (0.827–0.96)	0.888 (0.788–0.989)	0.884 (0.749–1.018)	0.881 (0.731–1.031)
	0.2	0.901 (0.892–0.91)	0.893 (0.849–0.938)	0.884 (0.793–0.974)	0.874 (0.736–1.013)	0.864 (0.676–1.052)	0.86 (0.65–1.069)
	0.3	0.9 (0.89–0.91)	0.889 (0.838–0.94)	0.875 (0.769–0.98)	0.86 (0.696–1.024)	0.845 (0.62–1.07)	0.838 (0.587–1.09)

Table A4. Median quasi-extinction times for each of the 54 epizootic scenarios. Range (minimum to maximum) quasi-extinction times are included in parentheses.

		μ					
ρ	f	0.01	0.05	0.1	0.15	0.2	0.3
–0.1	0.1	29 (28–30)	28 (27–29)	28 (27–29)	29 (28–30)	29 (28–30)	28 (27–29)
	0.2	28 (26–29)	27 (25–28)	25 (23–27)	28 (25–29)	26 (23–29)	25 (22–28)
	0.3	26 (24–29)	24 (21–27)	22 (19–26)	27 (22–30)	24 (19–29)	22 (17–27)
0.40	0.1	25 (22–29)	22 (18–26)	20 (16–24)	25 (18–30)	23 (16–29)	20 (14–26)
	0.2	24 (19–29)	21 (16–25)	18 (14–23)	24 (16–29)	21 (13–28)	18 (12–25)
	0.3	24 (20–29)	20 (16–25)	18 (15–22)	24 (17–29)	21 (14–28)	18 (12–25)
0.73	0.1	29 (28–30)	28 (27–29)	28 (27–29)	29 (28–30)	29 (28–30)	28 (27–29)
	0.2	28 (26–29)	27 (25–28)	25 (23–27)	28 (25–29)	26 (23–29)	25 (22–28)
	0.3	26 (24–29)	24 (21–27)	22 (19–26)	27 (22–30)	24 (19–29)	22 (17–27)

Appendix A5

Exploration of density-dependent force of infection

In many disease systems, force of infection (FOI) can be density-dependent, which in turn can profoundly influence disease transmission and population dynamics. In order to explore the potential population-level effects of density-dependent FOI, we repeated stochastic simulations (500 replicate runs of 5000 simulations for 50 years) using methods described in the text, except that the force of infection was allowed to be density-dependent, and estimated quasi-extinction parameters.

Modeling FOI as a density-dependent parameter requires a functional form of density-dependent effects on FOI, and estimates of parameters required for the density-dependent function. Ozgul et al. (2009) modeled FOI as a function of population size within a capture-mark-recapture modeling framework. We note that Ozgul et al. (2009) found no evidence that that population size substantially influenced FOI. Nonetheless, we explored the population-level consequences of density-dependent FOI by assuming that FOI was linearly affected by population size on a logit scale, and using estimates of logistic regression parameters for tortoise populations with high seroprevalence (Ozgul et al. 2009; A. Ozgul unpubl.). The table below lists the parameter estimates and standard errors:

	Estimate	Standard error	Lower 95% confidence limit	Upper 95% confidence limit
b_0 (intercept)	–1.4534	0.2899	–2.0217	–0.8851
b_1 (slope)	0.0342	0.0237	–0.0124	0.0808

At each time step, we modeled force of infection (ϕ) as a logistic function of the total population size at the previous time step (N_{t-1}) as:

$$\phi_t = \frac{\exp\left(b_0 + b_1 N_{t-1}\right)}{1 + \exp\left(b_0 + b_1 N_{t-1}\right)}$$

The parameters b_0 and b_1 represent logistic regression parameters used to quantify the effect of population density on force of infection as described above.

For each simulation, the population projection matrix (corresponding to a particular environmental state defined by the Markov chain model for a respective epizootic scenario) was parameterized vital rates sampled from their respective statistical distributions (as described in Supplementary material Appendix A3). At each time step t of each simulation, the force of infection was calculated based on total population size at time $t - 1$ as defined by the above equation, and incorporated into the projection matrix.

We repeated the analyses with density-dependent FOI for only two epizootic scenarios: (1) $\rho = -0.10$, $f = 0.10$, $\mu = 0.01$, and (2) $\rho = 0.73$, $f = 0.30$, $\mu = 0.30$, to capture the effects of density-dependent FOI under the two most extreme epizootic scenarios. We list the results of this analysis along with the results from our original analysis assuming density-dependent FOI for comparison.

Modeling force of infection as a density-dependent process only had marginal effect on estimates of quasi-extinction parameters, and did not alter our findings or conclusions.

Table A5. Estimates of probability of quasi-extinction ($\Pr\{T_q \leq 50\}$) and median extinction time (T_q50) when the force of infection (ϕ) was and was not modeled as a density-dependent parameter. Ninety-five percent confidence intervals also are given for the estimate of quasi-extinction parameters. Estimates of quasi-extinction parameters are given only for two epizootic scenarios. See text for details.

Epizootic scenario	Form of ϕ	$\Pr\{T_q \leq 50\}$ (95% CL)	T_{q50} (95% CL)
$\rho = -0.10, f = 0.10, \mu = 0.01$	Density-dependent	0.746 (0.732–0.759)	29 (28–30)
	Density-independent	0.749 (0.736–0.761)	29 (28–30)
$\rho = 0.73, f = 0.30, \mu = 0.30$	Density-dependent	0.971 (0.783–0.997)	17 (7–29)
	Density-independent	0.946 (0.798–0.993)	19 (10–29)

References

Aars, J. et al. 2001. Water vole in the Scottish uplands: distribution patterns of disturbed and pristine populations ahead and behind the American mink invasion front. – Animal Conservation, Scotland Univ. Aberdeen, Dept Zool., Aberdeen, AB24 2TZ, Scotland 4: 187–194.

Amstrup, S. C. et al. 2005. Handbook of capture–recapture analysis. – Princeton Univ. Press.

Berry, K. H. 2002. Using growth ring counts to age juvenile desert tortoises (*Gopherus agassizii*) in the wild. – Chelonian Conserv. Biol. 4: 416–424.

Brode, W. E. 1959. Notes on behavior of *Gopherus polyphemus*. – Herpetologica 15: 101–102.

Brown, D. R. 2002. Mycoplasmosis and immunity of fish and reptiles. – Front. Biosci. 7: 1338–1346.

Burnham, K. P. et al. 2002. Model selection and multimodel inference: a practical information-theoretic approach. – Springer.

Butler, J. A. et al. 1996. Reproduction of the tortoise, *Gopherus polyphemus*, in northeastern Florida. – J. Herpetol. 30: 14–18.

Caswell, H. 2001. Matrix population models. – Sinauer Ass.

Crouse, D. T. et al. 1987. A stage-based population model for loggerhead sea turtles and implications for conservation. – Ecology 68: 1412–1423.

Epperson, D. M. et al. 2003. Nesting and hatchling ecology of the gopher tortoise. – J. Herpetol. 37: 315–324.

Germano, D. J. 1988. Age and growth histories of desert tortoises using scute annuli. – Copeia 1988: 914–920.

Hunter, C. M. et al. 2005. The use of the vec-permutation matrix in spatial matrix population models. – Ecol. Modell. 188: 15–21.

Krebs, C. J. et al. 1995. Impact of food and predation on the snowshoe hare cycle. – Science 269: 1112–1115.

Landers, J. L. et al. 1980. Reproduction of gopher tortoises (*Gopherus polyphemus*) in southwestern Georgia. – Herpetologica 36: 353–361.

Lipsey, M. W. et al. 2001. Practical meta-analysis. – Sage Publications Inc.

Marshall, J. E. 1987. The effects of nest predation on hatchling gopher tortoises (*Gopherus polyphemus*). – Univ. of South Alabama.

McDonald, T. 2008. mra: analysis of mark–recapture data. (<http://cran.cnr.berkeley.edu/web/packages/mra/index.html>).

Mushinsky, H. R. et al. 1994. Growth and sexual dimorphism of *Gopherus polyphemus* in central Florida. – Herpetologica 50: 119–128.

Ozgul, A. et al. 2009. Upper respiratory tract disease, force of infection, and effects on survival of gopher tortoises. – Ecol. Appl. 19: 786–798.

Perez-Heydrich, C. 2010. Ecological investigations of mycoplasmal upper respiratory tract disease in natural populations of threatened gopher tortoises: insights from population ecology, mathematical epidemiology and behavioral ecology. – PhD thesis, Infectious diseases and pathology, College of veterinary medicine, Univ. of Florida.

Pike, D. A. et al. 2006. Variation in hatchling tortoise survivorship at three geographic localities. – Herpetologica 62: 125–131.

Wendland, L. D. et al. 2007. An improved ELISA for Mycoplasma agassizii exposure: a valuable tool in the management of environmentally sensitive tortoise populations. – Clin. Vaccine Immunol. 14: 1190–1195.

Williams, B. K. et al. 2001. Analysis and management of animal populations. – Academic Press.

Wilson, D. S. et al. 2003. Estimating age of turtles from growth rings: a critical evaluation of the technique. – Herpetologica 59: 178–194.

Wright, J. S. 1982. The distribution and population biology of the gopher tortoise, *Gopherus polyphemus*, in South Carolina. – Clemson Univ.